Vascular channels formed by subpopulations of PECAM1+ melanoma cells

Published in final edited form as:
Nat Commun. ; 5: 5200. doi:10.1038/ncomms6200.

Vascular channels formed by subpopulations of PECAM1+ melanoma cells

James M. Dunleavey[1], **Lin Xiao**[1], **Joshua Thompson**[1], **Mi Mi Kim**[1], **Janiel M. Shields**[2], **Sarah E. Shelton**[3], **David M. Irvin**[4], **Victoria E. Brings**[1], **David Ollila**[5], **Rolf A. Brekken**[6], **Paul A. Dayton**[3], **Juan M. Melero-Martin**[7], and **Andrew C. Dudley**[1,2,8]

[1]Department of Cell Biology & Physiology, The University of North Carolina at Chapel Hill, Chapel Hill, NC 27599

[2]Lineberger Comprehensive Cancer Center, Chapel Hill, NC 27599

[3]Joint Department of Biomedical Engineering, The University of North Carolina at Chapel Hill, Chapel Hill, NC 27599 and North Carolina State University, Raleigh, NC 27695

[4]Curriculum in Genetics & Molecular Biology, The University of North Carolina at Chapel Hill, Chapel Hill, NC 27599

[5]Department of Surgery, The University of North Carolina at Chapel Hill, Chapel Hill, NC 27599

[6]Departments of Surgery and Pharmacology, UT Southwestern Medical Center, Dallas, TX 75235

[7]Department of Cardiac Surgery, Harvard Medical School and Children's Hospital Boston, Boston MA 02115

[8]McAllister Heart Institute, Chapel Hill, NC 27599

Abstract

Targeting the vasculature remains a promising approach for treating solid tumors; however, the mechanisms of tumor neovascularization are diverse and complex. Here we uncover a new subpopulation of melanoma cells that express the vascular cell adhesion molecule PECAM1, but not VEGFR-2, and participate in a PECAM1-dependent form of vasculogenic mimicry (VM). Clonally-derived PECAM1$^+$ tumor cells coalesce to form PECAM1-dependent networks in vitro and they generate well-perfused, VEGF-independent channels in mice. The neural crest specifier AP-2α is diminished in PECAM1$^+$ melanoma cells and is a transcriptional repressor of PECAM1. Reintroduction of AP-2α into PECAM1$^+$ tumor cells represses PECAM1 and abolishes tube-forming ability whereas AP-2α knockdown in PECAM1$^-$ tumor cells up-regulates PECAM1

Correspondence: Dr. Andrew C. Dudley: acdudley@med.unc.edu.

Contributions

J.M.D. and A.C.D. designed experiments. J.M.D., L.X., J.T., M.K., D.M.I., V.E.B., and A.C.D. performed experiments. S.E.S. performed acoustic angiography experiments. J.M.S. performed microarray analysis of human melanoma cell lines. J.M.M. performed karyotype experiments. R.A.B., D.W.O., and P.A.D. contributed to experimental design and provided critical reagents. J.M.D and A.C.D wrote the manuscript. All authors have read and approved the final manuscript.

Competing Financial Interests

The authors declare no competing financial interests.

Accession Codes

Microarray data is available at the Gene Expression Omnibus, accession number: GSE59564.

expression and promotes tube formation. Thus, VM-competent subpopulations, rather than all cells within a tumor, may instigate VM, supplant host-derived endothelium, and form PECAM1-dependent conduits that are not diminished by neutralizing VEGF.

Keywords

Vasculogenic mimicry; tumor angiogenesis; tumor endothelial cells; melanoma; tumor microenvironment; tumor heterogeneity; anti-angiogenic therapy

Introduction

Solid tumors require blood vessels for growth, access to oxygen and nutrients, and the removal of waste products. Thus, Folkman proposed that anti-angiogenic therapies could be used to attack tumor-associated blood vessels and shrink solid tumors [1]. Anti-angiogenic therapies are typically designed to target vascular endothelial cells (EC) that form tumor blood vessels. Therefore, anti-angiogenic drugs should be active against a spectrum of cancers. Furthermore, unlike conventional cytotoxic chemotherapy which targets genetically unstable and heterogeneous tumor cells, anti-angiogenic therapies target the vasculature which theoretically will not acquire drug resistance but should respond predictably to angiogenesis inhibition.

Whereas numerous preclinical models have documented the successful use of angiogenesis inhibitors to block tumor growth, these studies collectively show that tumors are typically only growth delayed, rather than driven into dormancy [2–5]. Thus, the tumor vasculature may be more complex than previously considered and tumors may have secondary mechanisms for re-vascularization [6,7]. For example, freshly isolated tumor-specific EC (TEC) from different tumor types display multiple abnormalities [8–12]. Two tumor-specific modes of neovascularization including “transdifferentiation” of stem-like tumor cells and vasculogenic mimicry (VM) are also suggested [13–22]. These tumor cell autonomous routes to neovascularization may underlie some of the dysfunctional features of tumor blood vessels and create outlets for escape from angiogenesis inhibition.

VM, initially described in aggressive forms of uveal melanoma, has been documented in multiple tumor types and is correlated with poor patient survival [23]. Tumor cell-lined networks are typically identified in histological sections by periodic acid-Schiff staining of matrix-rich channels, which contain blood, with few or no EC present. However, the different molecular mechanisms that generate VM-competent tumor cells are unclear and how tumor cell-lined conduits are formed and connected with the host vasculature is undetermined. Furthermore, it remains controversial whether tumor cells actively engage tumor blood vessels in a process resembling EC-mediated angiogenesis or if tumor cells simply fill in gaps between neighboring EC in a passive, nonfunctional manner [24].

Bona fide TEC may be identified and isolated from collagenase-dispersed tumors using intercellular adhesion molecule-2 (ICAM2) or platelet endothelial cell adhesion molecule (PECAM1, also known as CD31) antibodies followed by immunomagnetic separation [8,25]. Using this methodology, we have uncovered a novel subpopulation of PECAM1^{+} tumor

cells in melanoma that participate in a PECAM1-dependent form of VM. Unlike previous models suggesting that tumor cells contribute to neovascularization through endothelial-like differentiation or recapitulation of developmental plasticity, we demonstrate that VM-competent tumor cells exist as stable, yet hidden subpopulations in heterogeneous melanomas [15,26,27]. Clean separation of PECAM1$^-$ and PECAM1$^+$ clonal populations from the same tumor has allowed us to compare and contrast the differential roles these two populations play during tumor growth, angiogenesis, and responses to anti-angiogenic therapy.

Results

Identification of PECAM1$^+$ tumor cells from B16F10 melanoma

Using PECAM1 immunomagnetic separation of collagenase-dispersed B16F10 melanoma allografts [8,28], we enriched a PECAM1$^+$ population to ~ 98% purity, as determined by flow cytometry (Fig. 1a, b). Compared to the PECAM1$^-$ fraction, the enriched PECAM1$^+$ population expressed abundant *Pecam1* mRNA by semi-quantitative RT-PCR (Fig. 1c). Unexpectedly, *VE-cadherin* mRNA was not detected in the PECAM1$^+$ fraction, in contrast to mouse dermal endothelial cells (mEC) used as a positive control (Fig. 1c) [8]. However, the PECAM1$^+$ fraction strongly expressed the melanocyte marker tyrosinase (*Tyr*) leading us to suspect we had enriched a previously unidentified PECAM1$^+$ subpopulation of melanoma cells from the B16F10 cell line. To test this possibility, we engrafted parental B16F10-GFP tumor cells into wild type, C57BL/6 mice and unlabeled B16F10 cells into C57BL/6-Tg$^{(CAG–EGFP)}$1Osb/J mice. We then used PECAM1 immunomagnetic separation to retrieve highly purified fractions as before. The results showed that B16F10-GFP tumor cells in a wild type host generated PECAM1$^+$/GFP$^+$ cells whereas wild type tumors in a GFP host generated PECAM1$^+$/GFP$^-$ cells (Fig. 1d). These results are consistent with a tumor cell-of-origin for the PECAM1$^+$ cells we have isolated. Furthermore, these results appear to rule out the possibility of fusion between tumor cells and PECAM1$^+$ vascular EC in this particular mouse tumor model.

Next, we determined the proportion of PECAM1$^+$ tumor cells in B16F10 tumors in vivo using flow cytometry. Tumors were harvested once they had reached ~ 0.4 g (+/− 0.26 g, s.e.m.) or ~ 1.0 g (+/− 0.22 g, s.e.m.) in size. The proportion of PECAM1$^+$ tumor cells remained at ~ 0.2% of the total cellular pool, irrespective of tumor size. After gating out CD45$^+$ hematopoietic cells, the ratio of PECAM1$^+$ vascular EC to PECAM1$^+$ tumor cells was approximately 10:1 (Fig. 1e, f). Taken together, these results suggest that subpopulations of melanoma cells may express the vascular cell adhesion molecule PECAM1 in vivo.

Isolation of PECAM1$^+$ clonal populations from B16F10 melanoma

PECAM1$^+$ cells comprised a minor fraction of B16F10 cultures and could not be easily detected by flow cytometry. However, occasional clusters of PECAM1$^+$ cells could be found under fluorescence microscopy when B16F10 cultures were directly stained with PECAM1 antibodies (Supplementary Fig. 1a). To further explore the significance and biological functions of PECAM1$^+$ melanoma cells, we prepared clonal populations using

limiting dilution assays from highly enriched PECAM1$^+$ fractions (Fig. 2a). In 50% enriched fractions, PECAM1$^+$ tumor cells were visible as large, flattened colonies that were distinct in appearance from spindle-shaped, PECAM1$^-$ tumor cells (Supplementary Fig. 1b). These PECAM1$^+$ tumor cells could be cleanly separated from their PECAM1$^-$ counterparts using cloning rings or multiple rounds of immunomagnetic separation with PECAM1 antibodies followed by limiting dilution assays. qPCR using clonally-derived populations revealed robust *Pecam1* mRNA expression in clones A2 and A5 but not in clone A1 (Fig. 2b). No mRNAs were detected for *VE-cadherin* or *Vegfr-2* in PECAM1$^-$ or PECAM1$^+$ tumor cells. *Tyr* was expressed by all melanoma cells but not mEC, as expected. Confocal microscopy revealed that PECAM1 was concentrated at the cell membrane in mEC but was diffusely localized at the membrane and throughout the cytoplasm in PECAM1$^+$ tumor cells (Supplementary Fig. 1c). Western blotting confirmed a migrating band at the expected size for murine PECAM1 in PECAM1$^+$ clones (Fig. 2c). PECAM1 was tyrosine phosphorylated in PECAM1$^+$ tumor cells suggesting it may have similar signaling abilities in both EC and tumor cells (Supplementary Fig. 1d).

PECAM1$^+$ melanoma cells generate PECAM1$^+$ progeny

We found that PECAM1 expression in PECAM1$^+$ clones was stable in vitro and was not diminished by growth in different culture media (Supplementary Fig. 2a). However, cell-surface PECAM1 was reduced by > 50% when PECAM1$^+$ tumor cells were detached from tissue culture dishes using trypsin as opposed to accutase which does not affect PECAM1 surface expression (Supplementary Fig. 2b). Additionally, routine passaging of cells did not diminish PECAM1 expression (Supplementary Fig. 2c). Interestingly, PECAM1$^+$ tumor cells displayed a slight growth delay in vitro and in vivo when engrafted into mice (Supplementary Fig. 2d). Long-term in vitro propagation of PECAM1$^-$ and PECAM1$^+$ tumor cells revealed that PECAM1$^+$ tumor cells generally give rise to PECAM1$^+$ progeny and vice versa (Supplementary Fig. 2e). To determine the fate of PECAM1$^-$ and PECAM1$^+$ tumor cells in vivo, we transduced PECAM1$^+$ and PECAM1$^-$ tumor cells with GFP using lentivirus to generate PECAM1$^+$/GFP$^+$ (clone A5) or PECAM1$^-$/GFP$^+$ (clone A1) lines. We then injected 1.0×10^6 tumor cells subcutaneously in wild type C57BL/6 mice. Flow cytometry of collagenase-dispersed tumors revealed that, in general, PECAM1$^+$ tumor cells generate PECAM1$^+$ progeny whereas PECAM1$^-$ tumor cells generate mostly PECAM1$^-$ progeny (Supplementary Fig. 2f). When quantified by flow cytometry, PECAM1$^-$ tumors generated a mixed population consisting of ~ 2% PECAM1$^+$ progeny and ~ 98% PECAM1$^-$ progeny. These results suggest that PECAM1$^-$ and PECAM1$^+$ melanoma cells are stable subpopulations but may generate their counterparts at low frequencies with a tendency for PECAM1$^-$ tumor cells to generate PECAM1$^+$ progeny. Finally, karyotypes performed on PECAM1$^+$ and PECAM1$^-$ clones showed that PECAM1$^-$ tumor cells were more variable in chromosome counts with a median chromosome number of 70 whereas PECAM1$^+$ tumor cells had a median chromosome count of 64 (Supplementary Fig. 3a, b). Both PECAM1$^-$ and PECAM1$^+$ clones displayed similar marker chromosomes to those observed in previously published reports of the B16 cell line [29,30]. This result, in addition to the shared chromosomal aberrations between the two populations, suggests that the PECAM1$^+$ fraction may have persisted and been continuously generated at a low frequency within the B16F10 cell line for decades.

In vitro vascular properties of PECAM^{+} melanoma

To further characterize established PECAM1^{+} clones, we carried out a microarray analysis using an Affymetrix mouse gene ST1.0 platform. A complete microarray dataset showing differentially expressed genes in PECAM1^{-} and PECAM1^{+} tumor cells has been uploaded to the Gene Expression Omnibus (GEO). Notably, microarray analysis showed an enrichment of additional candidate genes associated with known vascular functions in PECAM1^{+} clones (A2, A3, A4, A5) compared to parental B16F10 tumor cells. These genes included *Ephb4*, *Bmpr2*, *Pdgfa*, *Icam1 (CD54)*, *Thbs1*, *Bmp1*, *Rbpj1*, and *Notch2* (Fig. 2d). Expression of these genes was confirmed by qPCR (Supplementary Fig. 4 and see Supplementary Table 1 for a complete list of PCR primer sets).

Because PECAM1 is a cell adhesion molecule known to mediate in vitro tube formation of bona fide EC, we assessed whether PECAM1^{+} melanoma cells might also undergo in vitro tube formation [31,32]. PECAM1^{+} tumor cells displayed a 4–5 fold increase in branching tube-like networks compared to their PECAM1^{-} counterparts. PECAM1^{-} tumor cells only formed occasional tube-like structures which were not stable in culture. Tube like-structures in PECAM1^{+} tumor cells could be inhibited by ~ 50% using a PECAM1 blocking antibody indicating a functional role for PECAM1 in this assay (Fig. 2e) [33]. Gain of function experiments showed that PECAM1 over-expression (OE) in PECAM1^{-} tumor cells (clone A1) stimulated in vitro tube formation ~ 4-fold whereas PECAM1 shRNA in PECAM1^{+} tumors cells (clone A5) diminished tube formation by ~ 50% (Fig. 2f, g, h, i). These results suggest that PECAM1 is a marker of a unique subpopulation of B16F10 tumor cells and it plays a functional role in the establishment and stability of in vitro tube-like networks.

PECAM1^{+} tumor cells exist in spontaneous murine melanoma

Next, we turned to the ΔBraf/Pten−/− genetically-engineered mouse model of melanoma to assess whether PECAM1^{+} tumor cells were present in spontaneous tumors (Fig. 3a) [34]. First, we measured *Pecam1* mRNA expression using qPCR in two cell lines recently derived from tumors in ΔBraf/Pten−/− mice [35]. The results showed that *Pecam1* mRNA levels were above the zero transcript threshold we established using a known PECAM1^{-} clone derived from B16F10 (clone A1) (Fig. 3b). These results suggested that, similar to B16F10, a minor subpopulation of PECAM1^{+} tumor cells might be present within ΔBraf/Pten−/− tumor cells. To address this possibility, we used PECAM1-mediated immunomagnetic enrichment in PBT2460 tumor cells and found that after six enrichment steps, about 15% of the population expressed PECAM1 on the cell surface by flow cytometry. After two additional enrichment steps, about 98% of the population expressed PECAM1 (Fig. 3c). qPCR confirmed an ~ 100-fold increase in *Pecam1* mRNA in the enriched fraction when compared to the un-enriched parental population but *VE-cadherin* and *Vegfr-2* were absent from both populations (Fig. 3d). Notably, these PECAM1^{+} cells derived from ΔBraf/Pten−/− tumors were not identical to those obtained from B16F10; namely, unlike PECAM1^{+} cells from B16F10 melanoma, they did not express ICAM1 protein or mRNA by qPCR (Supplementary Fig. 5a, b).

Using the enriched PECAM1^{+} fraction from ΔBraf/Pten−/− tumors, we generated single-cell clones by limiting dilution assays. Similar to PECAM1^{+} tumor cells derived from B16F10,

single cell clones derived from ΔBraf/Pten−/− tumors maintained PECAM1 expression in culture that was detectable on the cell surface by flow cytometry (Fig. 3e). Furthermore, clonally-derived PECAM1$^+$ tumor cells from ΔBraf/Pten−/− tumors showed a five-fold increase in the formation of vascular-like networks in vitro compared to their PECAM1$^-$ counterparts (Fig. 3f). As with B16F10-derived PECAM1$^+$ tumor cells, these tube-like structures were stable over time but could be diminished by ~ 50% using a PECAM1 neutralizing antibody (Fig. 3g, Supplementary Movie 1).

PECAM1$^+$ melanoma cells integrate into vessel lumens in vivo

To assess whether PECAM1$^+$ melanoma cells generated vessel-like structures in vivo, we engrafted unlabeled, clonally-derived PECAM1$^+$ (clone A5) and PECAM1$^-$ (clone A1) melanoma cells under the skin of C57BL6/J mice. We then stained cryosections with antibodies against PECAM1 and the melanoma marker S100B [36]. Strikingly, in PECAM1$^+$ tumors, we found intra-tumoral holes and channels lined by PECAM1$^+$/S100B$^+$ tumor cells (Fig. 4a). These channels appeared to be formed entirely by PECAM1$^+$/S100B$^+$ tumor cells (top row) or were formed in collaboration with PECAM1$^+$/S100B$^+$ tumor cells and host endothelium (middle row). In contrast, PECAM1$^-$ tumors were characterized by host-derived PECAM1$^+$ vasculature juxtaposed to S100B$^+$ tumor cells (bottom row). Next, we used GFP-labeled PECAM1$^+$ and PECAM1$^-$ clonally-derived populations from B16F10 to further assess the localization of PECAM1$^-$ and PECAM1$^+$ tumor cells in vivo by immunohistochemistry. Similar to the results above, in PECAM1$^+$ tumors, co-staining using PECAM1 and GFP antibodies revealed large openings, intratumoral channels, and vascular-like structures that incorporated GFP$^+$ tumor cells within their lumens (Fig. 4b, first row). In contrast, host-derived PECAM1$^+$ vascular EC were mainly peripheral to GFP$^+$ tumor cells in PECAM1$^-$ tumors (Fig. 4b, second row). We then determined whether PECAM1$^+$ tumor cells were also incorporated into VE-cadherin$^+$ vascular lumens. Similar to the staining pattern for PECAM1 above, we found that PECAM1$^+$ tumor cells formed mosaic vascular structures and were incorporated within occasional VE-cadherin$^+$ lumens (Fig. 4b, third row). In contrast, PECAM1$^-$ counterpart tumor cells were localized to the margins of host-derived VE-cadherin$^+$ blood vessels (Fig. 4b, fourth row). Taken together, these results suggest that PECAM1$^+$ melanoma cells have vascular-like properties including the ability to spontaneously organize into tube-like structures in vitro and incorporate into vascular lumens in vivo.

PECAM1$^+$ melanoma form perfused vascular structures in mice

To determine whether PECAM1$^+$ tumor cells were in direct contact with the host circulation, we examined paraffin-embedded tumor sections stained with GFP antibodies visualized using 3,3′ diaminobenzidine (DAB). The results showed numerous channels or “lumens” that were comprised of GFP$^+$ tumor cells in direct contact with erythrocytes (Fig. 5a). H & E stained sections showed large dilated vessels, hemorrhage, and blood-filled channels in PECAM1$^+$ tumors versus their PECAM1$^-$ counterparts (Fig. 5b). When quantified using the ImageJ software package, the mean hemorrhage area for PECAM1$^-$ tumors was 46.7 AU +/− 1.3 and 88.3 AU +/− 23.0 for PECAM1$^+$ tumors (Fig. 5b, lower panel). In support of a PECAM1-dependent form of VM in this model, this increase in

hemorrhage area was diminished when PECAM1$^+$ tumors were engrafted in PECAM1 KO mice (Supplementary Fig. 6a, b, c).

Next, we carried out 3D acoustic angiography and dynamic contrast-enhanced perfusion imaging using lipid-encapsulated micro-bubble contrast agents to measure real-time tumor perfusion and vascular structure in PECAM1$^-$ and PECAM1$^+$ tumors (Fig. 5c, left) [37]. Dual-frequency, 3D acoustic angiography revealed mean volumetric vascular density values of 47.9 +/− 2.9 for PECAM1$^-$ tumors, whereas PECAM1$^+$ tumors had mean volumetric vascular density values of 72.3 +/− 5.5 (Fig. 5c, middle). The sample means were statistically significant when analyzed using a two tailed t-test. We observed that the acoustic angiography images showed the presence of greater sub-resolution contrast in PECAM1$^+$ compared to PECAM1$^-$ tumors. This sub-resolution contrast signal likely emanates from pooling blood, which could correspond with the larger hemorrhage areas observed in PECAM1$^+$ tumors. Additionally, destruction-reperfusion images acquired longitudinally were used to compute the area-normalized relative blood volume (normalized RBV) analyzed using a linear mixed effects model in R. The area-normalized RBV regression intercept was 3.46 +/− 2.95 units for PECAM1$^-$ tumors and 15.60 +/− 4.76 units for PECAM1$^+$ tumors which was statistically significant (Fig. 5c, right). Overall, these results demonstrate that the normalized RBV of PECAM1$^+$ tumors was an average of 4.5 times higher than that of PECAM1$^-$ tumors.

To determine whether PECAM1$^+$ tumor cells were in contact with the circulation, we injected Texas Red-labeled high molecular weight Dextran (TR-Dextran) by way of the tail vein in mice bearing PECAM1$^-$/GFP$^+$ or PECAM1$^+$/GFP$^+$ tumors [38]. GFP$^+$ tumor cells in direct contact with TR-Dextran were then analyzed using confocal microscopy (Fig. 5d). After analyzing multiple sections from 3–4 mice/group, we found a six-fold increase in PECAM1$^+$ tumor cells in contact with TR-Dextran when compared to their PECAM1$^-$ counterparts. These results were confirmed in an additional PECAM1$^+$ clone (clone A2) (Supplementary Fig. 7a, b, Supplementary Movies 2, 3). Finally, we carried out transmission electron microscopy (TEM) of engrafted PECAM1$^-$ and PECAM1$^+$ tumors. The ultrastructure of vessels in these tumors showed melanoma cells (identified by the presence of melanosomes, a unique feature of melanocytes and melanoma cells) in direct contact with the basal lamina of erythrocyte-containing vessels in PECAM1$^+$ tumors, but this contact was rarely seen in PECAM1$^-$ tumors (Supplementary Fig. 8). Thus, these results suggest that PECAM1$^+$ tumor cells organize into primitive vascular channels that may be affiliated with the host circulation and perfused with blood.

AP-2α is reduced in PECAM1$^+$ tumor cells and represses PECAM1

Next, we asked how PECAM1 expression was transcriptionally-regulated in PECAM1$^+$ tumor cells. Notably, we did not find evidence for epigenetic regulation of *Pecam1* expression in B16F10 because neither the DNA methyltransferase inhibitor 5-azacytidine nor the pan-HDAC inhibitor TSA could induce *Pecam1* mRNA (Supplementary Fig. 9a). However, PECAM1 is known to be regulated by the transcription factor GATA2 and additional binding sites in the PECAM1 promoter for SP1, ETS, and AP-2α are also reported [39]. We scanned the PECAM1 promoter and used semi-quantitative RT-PCR to

measure the expression of these candidate transcription factors in PECAM1^{-} and PECAM1^{+} clones. The results showed that unsorted B16F10 melanoma and clonally-derived PECAM1^{-} or PECAM1^{+} tumor cells either did not express or expressed similar levels of most of these transcription factors, including *Ets* (Fig. 6a). On the other hand, *Ap-2α* expression was strikingly diminished in PECAM1^{+} tumor cells and mEC but was expressed in unsorted B16F10 cells and PECAM1^{-} tumor cells. *Ap-2α* expression was similar in parental B16F0, the low-metastatic B16 clone B16F1, B16F10, and two independent PECAM1^{-} clones (Supplementary Fig. 9b). Expression of the well-characterized melanoma markers dopachrome tautomerase (*Dct)* and micropthalmia-associated transcription factor (*Mitf-m)* were also similar in these same cell lines at the mRNA and protein levels (Supplementary Fig. 9b, c). Interestingly, PECAM1^{+} clones consistently produced more pigmented cells in vitro and highly pigmented tumors in vivo despite expressing similar levels of *Tyr* and *Dct* compared to PECAM1^{-} counterparts (Supplementary Fig. 9d, e).

Because AP-2α levels were inversely correlated with PECAM1, we hypothesized that AP-2α might function as a transcriptional repressor of PECAM1. We used chromatin immunoprecipitation (ChIP) to confirm that AP-2α occupied the PECAM1 promoter in B16F10 tumor cells. Immunoprecipitation with an AP-2α antibody followed by PCR using two primer sets unique to the mouse PECAM1 promoter revealed amplified fragments of the predicted sizes (Fig. 6b). Furthermore, PECAM1^{-} tumor cells transfected with *Ap-2α* siRNA revealed up-regulation of *Pecam1* mRNA and protein expression, which was accompanied by a four-fold increase in tube formation in Matrigel (Fig. 6c, d). On the other hand, stable lentiviral re-expression of *Ap-2α* into PECAM1^{+} tumor cells resulted in down-regulation of *Pecam1* mRNA and protein expression, and a 6-fold reduction in tube formation (Fig. 6e, f, Supplementary Movie 4). These results suggest that AP-2α may repress PECAM1 expression and that diminished expression of AP-2α in PECAM1^{+} B16F10 cells accompanies their ability to form vascular like structures in vitro.

PECAM1^{+} tumor cells are enriched after anti-VEGF therapy

Because PECAM1^{+} tumor cells do not express VEGFR-2, but engage in VM, we hypothesized they might form VEGF-independent intratumoral channels in mice. First, we subjected mice bearing B16F10-GFP tumors to MCR84, a neutralizing antibody raised against VEGF-A, and then harvested tumors once they become refractory to further treatment (Fig. 7a) [40,41]. MCR84-treated mice demonstrated a characteristic delay in tumor growth, followed by tumor regrowth that was resistant to further VEGF inhibition (Fig. 7b). We then used flow cytometry to measure the proportion of GFP^{+}/PECAM1^{+} tumor cells in size-matched tumors. We found that in size-matched, MCR84-resistant tumors, the number of PECAM1^{+} tumor cells was enriched ~ 6 fold whereas PECAM1^{-} tumor cells and bona fide EC were marginally reduced (Fig. 7c, d). To examine the specific role of PECAM1^{+} tumor cells in tumor responses to anti-angiogenic therapy, we engrafted GFP-labeled clonally-derived populations of either PECAM1^{+} or PECAM1^{-} tumor cells into C57BL6/J mice. Mice were then treated with MCR84 as described above. We found that PECAM1^{-} tumors demonstrated an expected delay in tumor growth and reduction in tumor volume (~ two-fold decrease in tumor volume at day 15) when challenged with MCR84. On the other hand, PECAM1^{+} tumors showed no appreciable growth inhibition compared to controls

(Fig. 7e). H & E and GFP-stained tissue sections revealed striking differences in blood vessel morphology and numerous blood-filled "channels" encapsulated by GFP^+ tumor cells in the $PECAM1^+$ tumors challenged with MCR84 (Fig. 7f). Taken together, VEGF blockade induces expansion of a minor subpopulation of $PECAM1^+$ melanoma cells; furthermore, $PECAM1^+$ melanoma cells form tumors that do not respond to VEGF inhibition and they generate aberrant vascular-like structures following challenge with VEGF blocking antibodies.

Human melanoma contains a $PECAM1^+$ subpopulation

We examined *PECAM1* expression from microarray data generated from > 40 human melanoma cell lines and normal human melanocytes [42]. From these data, we identified approximately 10 cell lines which fell above a threshold (~ 1.5 adjusted mean fluorescence values from microarray data) established using normal human melanocytes which do not express *PECAM1* (Fig. 8a). A list of normal melanocytes and melanoma cells along with the raw fluorescence values from the microarray are shown in Supplementary Table 2. We began by culturing some of the highest *PECAM1*-expressing cell lines and measuring *PECAM1* mRNA levels by quantitative RT-PCR. The results showed that, as predicted from the microarray analysis, *PECAM1* mRNA was detected in the WM2664, MEL505, RPMI7951, WM1158, and SBCl2 cell lines albeit at vey low levels compared to human EC (hEC) (Fig. 8b). No *PECAM1* transcripts were detected in normal melanocytes, RPMI8332, or SKMEL119 which all fell below the established threshold on the microarray. On the other hand, *VE-CADHERIN* mRNA, which is expressed in some uveal forms of melanoma that engage in vasculogenic mimicry, was not detected in most cell lines but was found at very low levels in WM1158 cells [43]. Using flow cytometry, we could detect a minor shift in PECAM1 fluorescence in RPMI7951 (3.3%) and WM1158 cells (1.6%) but a much larger shift in SBCl2 cells (50%). No PECAM1 surface expression was detected in normal melanocytes (NHM7) or in RPMI8332, as expected (Fig. 8c). Similar to the $PECAM1^+$ fractions derived from murine B16F10 and ΔBraf/Pten−/− cells, SBCl2 melanoma cells formed robust and stable vessel-like networks in vitro which were inhibited by PECAM1 neutralizing antibodies (Fig. 8d, Supplementary Movie 5).

Because SBCl2 expressed detectable PECAM1 levels by flow cytometry, we engrafted this cell line subcutaneously in NOD-SCID-γ (NSG) mice. We then stained primary, paraffin-embedded SBCl2 tumors with PECAM1 antibodies that were verified to be human specific using western blotting and immunohistochemistry (Supplementary Fig. 10a, b). While the majority of $PECAM1^+$ tumor cells detected with human antibodies appeared randomly scattered throughout the tumor, occasional $PECAM1^+$ "lumens" were also visible (Fig. 8e). Overall, $PECAM1^+$ tumor cells were found at the luminal and abluminal surface of vascular structures (white arrowheads), and were detected in all SBCl2 tumors examined, and were present at an average density of ~ 5 vessel-like structures per mm^2 when normalized to tumor size for each tissue section (Fig. 8e, far right). Thus, similar to mouse melanoma, a subpopulation of some human melanoma cells express PECAM1 and engage in the formation of vascular-like structures in vitro and in vivo.

Discussion

We have identified a subpopulation of PECAM1$^+$ melanoma cells that was "hidden" within heterogeneous and predominantly PECAM1$^-$ melanoma tumors. Generally, PECAM1$^+$ melanoma cells were more motile and coalescent in Matrigel which could be reversed by introduction of the AP-2α transcription factor. However, PECAM1 expression was only partially repressed upon AP-2α introduction, indicating additional factors regulate PECAM1 expression in melanoma cells. Furthermore, the nature of the AP-2α defect in PECAM1$^+$ tumor cells is not yet clear and its diminished expression in these cells could be due to mutations, epigenetic silencing, or other unknown mechanisms. AP-2α is a putative tumor suppressor shown to act as a transcriptional repressor of melanoma cell adhesion molecule (*MCAM*) and activator of *KIT* [44,45]. AP-2α also controls melanoma cell motility and its expression is diminished in aggressive forms of melanoma and breast cancer [46,47]. Consistent with a role for AP-2α in cellular movement, we found that introduction of AP-2α into PECAM1$^+$ tumor cells completely blocked in vitro tube formation, a process involving cellular migration and stable intercellular connections.

PECAM1$^+$ tumor cells were present within the B16F10 population in low abundance, and we were unable to detect PECAM1 expression in the low-metastatic B16 clone B16F1. However, it is possible that an infrequent population of VM-competent tumor cells could also be enriched from these cell lines in nascent tumors or at sites of metastasis. For example, a minor population of PECAM1$^+$ tumor cells could assist during initial tumor neovascularization (when tumors are relatively small and have yet to recruit an efficient blood supply) by forming transient vascular channels that conduct blood or fluid. Remarkably, this concept was first suggested over 40 years ago in studies using melanoma transplants in the hamster cheek pouch [48]. It is also possible that not all "channels" formed by PECAM1-lined structures contain flowing blood and may thus resemble "blood lakes" described previously [49]. Whether or not these "blood lakes" are inert reservoirs or play an active, pathophysiological role in tumor progression remains unclear. VM-competent tumor cells could also be generated due to selection pressure (differentiation from PECAM1$^-$ counterparts) or mobilized in tumors challenged with angiogenesis inhibitors. Indeed, we found an ~ 6-fold enrichment of PECAM1$^+$ tumor cells in B16F10 tumors challenged with the VEGF blocking antibody, MCR84. PECAM1$^+$/VEGFR-2$^-$ tumor cells could therefore supplant vascular EC lost following treatment with anti-angiogenic therapy and form PECAM1-dependent "bridges" between neighboring tumor cells and EC (Fig. 9a, b).

We found that PECAM1 blocking antibodies could reduce the tube forming ability of PECAM1$^+$ tumor cells as they do in cultured EC [31]. Notably, PECAM1 introduction into mesothelioma cells (which do not express PECAM1) also induces robust tube formation in Matrigel [32]. PECAM1 is required for tube formation in bona fide EC, whereas VE-cadherin mediates both cell-cell adhesion and vacuole fusion [50]. Thus, PECAM1 expression in melanoma may mediate cell elongation, migration, and invasion while stabilizing the junctional, homophilic complexes between neighboring cells necessary to create a patent lumen [51]. Taken together, our model is rather different from a passive process of tumor cell-to-EC mosaicism observed in other tumor types [52,53]. Instead, co-option of PECAM1 by tumor cells may actively stabilize cell-cell interactions between PECAM1$^+$ tumor cells and

between PECAM1$^+$ tumor cells and EC. PECAM1 is typically concentrated at cell-cell borders by a process known as “diffusion trapping” which leads to cell aggregation where two PECAM1$^+$ cells meet [54]. Indeed, homophilic PECAM1-PECAM1 binding was suggested, many years ago, to mediate in vitro tumor cell adhesion to EC in co-culture studies [55].

Given the role of PECAM1 in mediating diapedesis (transendothelial migration) by inflammatory cells, it may be interesting to revisit recent studies demonstrating distinct mechanisms of metastasis using the B16F10 model to determine if subpopulations of PECAM1$^+$ tumor cells are involved [56]. We found PECAM1 tyrosine phosphorylation in melanoma cells, suggesting PECAM1-mediated signal transduction could function analogously in EC and in PECAM1$^+$ melanoma cells. In support of this possibility, clonal populations of PECAM1$^+$ melanoma displayed a slight growth delay compared to PECAM1$^-$ counterparts suggesting that PECAM1-PECAM1 interactions between tumor cells could stimulate contact inhibition, as it does in EC, and a slower rate of growth despite their ability to form vascular-like channels in vivo. It is therefore possible that acquisition of vascular-like characteristics by tumor cells could come at the expense of reduced tumorigenicity overall. Taken together, the PECAM1$^+$ population of melanoma cells we have uncovered could play multiple roles in diverse processes related to melanoma development, dormancy, migration/invasion, and angiogenesis.

Methods

Mice

For studies using the B16F10 melanoma cell lines, female C57BL6/J mice were used (Jackson Laboratories, Bar Harbor, ME). Mice were injected with tumor cells at 7–8 weeks of age. For engraftment of human melanoma cells, we used female NSG mice (7–8 weeks of age) provided by the mouse phase I unit at UNC. C57BL/6-Tg $^{(CAG-EGFP)}$1Osb/J mice were purchased from Jackson Laboratories, Bar Harbor, ME). *Pecam1* knockout mice were kindly provided by Dr. E. Tzima (UNC Chapel Hill), and tumor cells were engrafted in female mice at 7–8 weeks of age. All mouse experiments were carried out in accordance with protocols approved by the Institutional Animal Care and Use Committee at the University of North Carolina at Chapel Hill.

Cell lines and media

B16F0, B16F1, B16F10 (ATCC), ΔBraf/Pten−/− (derived from B6.Cg-Braf^{tm1Mmcm}Pten^{tm1Hwu}Tg$^{(Tyr-cre/ERT2)}$13Bos/BosJ mice (UNC-Chapel Hill Mouse Phase 1 Unit)) cell lines PBT2460 and PBT2130 (Drs. W. Kim and J. Bear, UNC-Chapel Hill), and human melanoma cell lines WM1158, SBCl2, Sk-Mel-119, Sk-Mel-173, and WM2664 (Dr. J. Shields, UNC-Chapel Hill) were maintained in DMEM with 4.5 g/mL D-Glucose and 10% FBS. Human melanoma cell lines RPMI7951, RPMI8322, and Mel505 (Dr. J Shields, UNC-Chapel Hill) were maintained in RPMI with 10% FBS. The normal human melanocyte line NHM7 (Dr. J Shields, UNC-Chapel Hill) was maintained in Media 254 (Gibco) supplemented with HGMS (Gibco). EC (isolated by us previously [8]) were maintained in

Endothelial Cell Media (EC-Media), composed of DMEM with 1g/L glucose, 5 μg/L bFGF, 10 μg/L VEGF, 100 mg/L heparin, antibiotics, and 10% NuSerum IV (BD).

Antibodies

For a complete list of antibodies and dilutions used, please refer to Supplementary Table 3.

Western blotting

Whole cell lysates were prepared in radioimmunoprecipitation assay buffer (RIPA, Boston BioProducts), separated by SDS-PAGE at 100V using a Bio-Rad 4–20% TGX gel (Bio-Rad), blocked with 5% Milk-TBS-T for standard western blotting, 5% BSA for phospo-VEGFR2 blotting, and probed with antibodies overnight at 4°C. Peroxidase-conjugated secondary antibodies were incubated at RT for 1 hour, and bands were exposed with Western Lightning (PerkinElmer). Blots were imaged on a Fluorchem M (ProteinSimple). All antibodies and dilutions are presented in Supplementary Table 3. Uncropped western blots are presented in Supplementary Fig. 11.

Chromatin immunoprecipitation (ChIP)

ChIP experiments were performed using the ChIPit Express Kit (Active Motif) according to the manufacturer's instructions. 2 μg anti-AP-2α antibodies were used for immunoprecipitation and bound DNA was analyzed using two primer sets designed against the mouse PECAM1 promoter (for sequences see Supplementary Table 1).

siRNA Knockdown

Cells were plated at 2.0×10^5 cells/well in 6-well plates. siRNA SmartPools (Dharmacon) targeting *Ap- 2α* (M-062788-01-0005), *Pecam1* (TRC RMM4534-EG18613), or non-targeting controls (D-001206-13-05) were added to plates the next day according to the manufacturer's instructions at a concentration of 100 nM. Cells were allowed to grow for 48 hours before harvesting.

Isolation of PECAM1$^+$ tumor cells

Tumors were harvested and prepared for cell isolation as previously described by us [8,57]. In brief, tumors were minced in cold DMEM with 1 g/L glucose. Tumors were further digested using a mechanical tissue homogenizer (Miltenyi). Samples were incubated at 37°C with 5 ml Collagenase T2 (2 mg/ml, Worthington), 1 mL neutral buffered protease (2.5 U/ml, Worthington), and 75 μL deoxyribonuclease (1 mg/mL, Worthington) for 75 minutes. Red blood cells were lysed with 1X Pharmlyse B (BD PharMingen). Cells were suspended in FACS Buffer (degassed phosphate-buffered saline containing 2 mM EDTA and 0.5% BSA), Fc receptors were blocked with Fc Block (Miltenyi), and 10 μg PE-conjugated anti-PECAM1 antibodies were added for 20 minutes. Cells were washed and resuspended with anti-PE magnetic beads (Miltenyi) for 15 minutes. Cells were then washed and passed over a magnetic column, washed, and then eluted. Eluted cells were washed and plated in EC-Media. Cells were grown for several weeks, and the isolation was repeated until cultures reached ~ 99% PECAM1 positivity, at which point single cell clones were made by limiting dilutions.

Tumor dissociation and flow cytometry

Single cell suspensions were prepared either from whole tumors as described above or from detached cell cultures as previously described by us [57]. Briefly, cells were washed with PBS and detached using accutase (Sigma) and then labeled with fluorophore-tagged antibodies. Cells were then washed and fixed in FACS buffer containing 1% paraformaldehyde. Cells were analyzed by flow cytometry using an Accuri C6 flow cytometer running BD Accuri CFlow Plus Analysis software. Samples were then analyzed using the FloJo software package (version 10).

Immunohistochemistry

Tumors were harvested and fixed in 4% paraformaldehyde overnight at 4°C. Samples were then cryoprotected in 30% sucrose overnight. Samples were frozen in OCT and cut into 7 μm sections. Slides were fixed in methanol for 20 minutes, and washed in PBS. Sections were blocked in 5% BSA with species-specific serum (5%) for one hour, and antibodies were added in blocking buffer. All antibodies and dilutions are described in Supplementary Table 3. Slides were incubated overnight at 4°C. Slides were washed and secondary antibodies were added for one hour at room temperature. Slides were counterstained with Vectashield Hard-set Mounting Medium with DAPI (Vector Labs). Sections were analyzed on a Leica DM-IRB inverted microscope or a Zeiss 710 laser scanning confocal microscope. Images were globally adjusted using ImageJ analysis software (http://rsb.info.nih.gov/ij) to enhance contrast and sharpness.

Acoustic angiography and perfusion imaging

Two methods of contrast enhanced ultrasonography were employed to quantify perfusion in PECAM1$^+$ and PECAM1$^-$ tumors in vivo. Additionally, non-contrast ultrasound provided reference anatomical information and tumor volume. The lipid encapsulated microbubble contrast agents were prepared with a (9:1) molar mixture of 1,2-distearoyl-sn-glycero-3-phosphocholine (DSPC, Avanti Polar Lipids, Alabaster, AL), and 1,2-distearoyl-*sn*-glycero-3-phosphoethanolamine-N-methoxy(polyethylene glycol)-2000] (mPEG-DSPE, Creative PEGWorks, Winston Salem, NC) in phosphate-buffered saline containing 15% (v/v) propylene glycol, and 5% (v/v) glycerol. Air in the headspace (1.5mL in a 3 mL vial) was exchanged with decafluorobutane (SynQuest Labs, Alachua, FL), and microbubbles were created by agitation with a Vialmix mixer (Bristol-Myers Squibb Medical Imaging, North Billerica, MA) [58]. Activated microbubbles were diluted and injected intravenously through a tail-vein catheter at a rate of 2.8×10^7 bubbles/min. Destruction-reperfusion imaging was performed using a Vevo 2100 ultrasound system (VisualSonics, Toronto, Ontario, Canada) and dynamic contrast enhanced perfusion imaging sequences were used to compute relative blood volumes (VevoCQ-Advanced Contrast Quantification Software Analysis Tool for the Vevo 2100. VisualSonics, Toronto, Canada, © Bracco Suisse S.A. 2010) [59]. Data were normalized by tumor cross-sectional areas as defined by regions of interest (ROIs) drawn manually. Acoustic angiography utilizes a prototype dual-frequency transducer, with a low frequency element to transmit at 4 MHz, exciting microbubbles to produce broadband, superharmonic echoes (at a mechanical index of 0.6). The confocal high frequency element (30 MHz) is used to receive the microbubble response, thus avoiding

tissue signal and producing high-contrast, high resolution images of the tumor microvasculature without tissue background, in 3 dimensions [37]. Acoustic angiography is acquired near simultaneously with b-mode soft tissue imaging, which provides anatomical reference. These images were used to compute the volumetric vascular density of the tumors using the following procedure in MATLAB (The MathWorks Inc., Natick, MA). First, ROIs were drawn manually to define tumor boundaries based on the b-mode images. Then, the ROIs were applied to mask the tumor volume in the acoustic angiography images. Finally, the vascular volume was computed by applying an intensity threshold cutoff, to segment the image into vascular and nonvascular regions. The volumetric vascular density is the ratio of the number of voxels classified as vascular volume over the total number of voxels in the tumor ROI. Statistical analysis was carried out using R (http://www.R-project.org).

Transmission electron microscopy

PECAM1$^+$ or PECAM1$^-$ tumors were grown as described above. Tissues were harvested, fixed in 2.5% glutaraldehyde/2% PFA in 0.15M sodium phosphate buffer. Samples were post-fixed for 1 hour in 1% osmium tetroxide in 0.15M sodium phosphate buffer, dehydrated with a graded series of ethanol washes, treated with propylene oxide and embedded in PolyBed 812 epoxy resin (Polysciences, Warrington, PA). Ultrathin sections (70–80 nm) were cut and mounted on copper grids and stained with 4% aqueous uranyl acetate and Reynolds' lead citrate. Sections were mounted to copper grids, OsO_4 was used to stain the tissues and sections were imaged on a Zeiss Leo EM910 TEM.

Lentiviral constructs and transduction

All recombinant DNA work was carried out under approval of the Environmental Health Safety Division of UNC-Chapel Hill. Lentiviral expression plasmids were created by E. Campeau and obtained from Addgene: pLenti CMV-GFP-DEST (736-1, Addgene plasmid 19732), pLenti CMV/TO GFP-Zeo DEST (719-1, Addgene 17431). Packaging plasmids psPax2 and pMD2.6 were created by Didier Trono (Addgene plasmids 12259 and 12260). Mouse ORF-eome constructs were acquired from the ATCC I.M.A.G.E Consortium, then cloned into pDONR 221 (Invitrogen) Gateway donor vectors using Clonase BP (Invitrogen). Cloned pDONR 221 vectors were sub-cloned into lentiviral expression vectors by Clonase LR reaction (Invitrogen). Lentiviral backbones were transfected with 1.5 μg packaging plasmids psPAX2 and pMDG2 with 15 μl Lipofectamine 2000 in 6-well plates into HEK293T cells. Viral particles were harvested at 24 and 48 hours post transfection. Viral particles were used to infect target cells with 10 μg/mL Polybrene in antibiotic-free media.

Tumor studies in mice

B16F10 melanoma cells were grown in appropriate culture medium, detached and resuspended in HBSS (Gibco). 1.0×10^6 tumor cells were injected subcutaneously in the right shoulder of C57BL6/J mice. Tumors were allowed to grow to 1 cm^3 and were measured daily with calipers. For MCR84 studies, mice were treated intraperitoneally every other day with 25 mg/kg/day MCR84 or isotype control antibodies as previously described [41,60]. Tumor sizes were measured with calipers each day. At the end of the experiment, mice were euthanized and tumors were harvested and weighed.

Microarray analysis

RNA was harvested from cell lines and run on a Mouse Gene ST1.0 Chip (Affymetrix). Heat maps were generated using the Gene-E software package, version 2.1.134. (http://www.broadinstitute.org/cancer/software/GENE-E/).

Polymerase chain reaction (PCR)

Primers were designed using Invitrogen Primer Perfect Design Software. End-point PCR was completed using a standard PCR kit (NEB). RT-qPCR was completed with Maxima SYBR Green (ThermoFisher) on an Applied Biosystems Step One Plus analyzer. All qPCR experiments were run in triplicate and data are presented as the average with the standard error of the mean (s.e.m.). Primer sequences used are presented in Supplementary Table 1.

Tumor hemorrhage quantification

H & E stained sections were imaged using polarized light microscopy which caused red blood cells (RBC) to fluoresce. Images were subsequently converted to a binary image using ImageJ software. The images were then thresholded to only show RBC and the “count particles” tool was used to analyze RBC content. The first 500 observations were binned and plotted.

In vitro tube-forming assays

Briefly, 50 μL Matrigel (BD) was plated in 96-well culture dishes and allowed to polymerize at 37°C for 30 minutes. Next, 2.5×10^4 cells/well were plated on the Matrigel layer and grown for 16 hours. Randomized fields were captured using a DM-IRB inverted microscope and tubes were quantified from each image. Data are presented as the average number of tubes per field +/− s.e.m. from multiple fields. For live imaging experiments Matrigel was plated in 24-well plates, and 5×10^4 cells/well were seeded on top of the layer. Tube formation was imaged on a Leica IX70 microscope outfitted with an environmental chamber. Data were compiled using ImageJ Analysis Software. Brightfield images were converted to eight-bit black and white and the “find edges” command was used to identify cells. Images were enhanced using sharpen tools and pseudocolored for video analysis.

Dextran perfusion

Dextran perfusion was carried out according to previously published methods [38]. GFP labeled tumor cells were injected subcutaneously as described. Once tumors reached 1 cm^3, mice were injected with 100 μL, 70 kD-Texas Red Dextran (Life Technologies) via the tail vein and sacrificed three minutes post-injection. Tumors were prepared for immunohistochemistry as described and imaged with a Zeiss LSM700 scanning laser confocal microscope. Tumor-cell affiliated dextran was quantified by identifying GFP^+ cells abutting on dextran-lined channels in tumors and are presented as average tumor cells integrated within lumens per field.

XTT Assay

XTT Assay Kit (ATCC) was used to measure growth of cells. 5,000 cells were plated in triplicate in a 96 well plate. XTT reagent was prepared per manufacturers recommendations, added to wells, and absorbance at 475 nm was measured after 4 hours.

5-azacytadine (5-aza) and trichostatin A (TSA) treatment

5-Aza (stock: 819mM) or TSA (stock: 6.6mM) were diluted as indicated and added to media. Cells were harvested seven days later and RNA was purified for semi quantitative RT-PCR analysis.

Karyotypes

Cells were treated with 0.1 μg/mL colcemid (Irvine Scientific, Santa Ana, CA) for 3 hours to accumulate cells in metaphase. Cells were then treated with hypotonic 0.075M KCl for 25 minutes at 37°C and fixed in 3:1 methanol:acetic acid. Air-dried slides were stained for G-band analysis and at least 20 metaphase cells were counted for each cell line by the Brigham and Women's Hospital CytoGenomics Core Laboratory, Boston, MA.

Statistical analysis

Statistical power for mouse experiments was calculated using Biomath (biomath.info/power). All samples sizes were equal to or greater than recommended minimum group size. All measurements in mouse studies were done with the assistance of at least one blinded researcher for recording and confirmation. Statistical analysis was carried out using the Graphpad Prism 5.0f statistical analysis package unless otherwise noted. Figure legends list specific n and p values. Data are presented as mean ± standard error of the mean (s.e.m.).

Supplementary Material

Refer to Web version on PubMed Central for supplementary material.

Acknowledgments

A.C.D. is supported by grants from the National Institutes of Health (R00-CA140708 and R01-CA177875) and the University Cancer Research Fund at UNC Chapel Hill. J.M.D. is supported by a pre-doctoral fellowship (F31-CA174245) from the National Institutes of Health. We acknowledge NIH grant S10-OD010410 for the shared ultrasound instrumentation. We thank Kirk McNaughton and Ashley Ezzell in the Cell Biology and Physiology Histology Research Core and the UNC Microscopy Services Laboratory in the UNC Department of Pathology and Laboratory Medicine. We thank Drs. William Kim and James Bear at UNC Chapel Hill for sharing the mouse melanoma lines from ΔBraf/Pten−/− mice. Finally, we'd like to thank Dr. Eleni Tzima at UNC Chapel Hill for sharing the *Pecam1* KO mice.

References

1. Folkman J. Anti-angiogenesis: new concept for therapy of solid tumors. Ann Surg. 1972; 175:409–416. [PubMed: 5077799]
2. Cao Y, et al. Forty-year journey of angiogenesis translational research. Sci Transl Med. 2011; 3:114rv3.
3. Carmeliet P, Jain RK. Molecular mechanisms and clinical applications of angiogenesis. Nature. 2011; 473:298–307. [PubMed: 21593862]

4. Ellis LM, Hicklin DJ. Pathways Mediating Resistance to Vascular Endothelial Growth Factor-Targeted Therapy. Clinical Cancer Research. 2008; 14:6371–6375. [PubMed: 18927275]
5. Ellis LM, Fidler IJ. Finding the tumor copycat. Therapy fails, patients don't. Nat Med. 2010; 16:974–975. [PubMed: 20823880]
6. Dudley AC. Tumor endothelial cells. Cold Spring Harbor perspectives in. 201210.1101/cshperspect.a006536
7. Dunleavey JM, Dudley AC. Vascular mimicry: Concepts and implications for anti-angiogenic therapy. Current Angiogenesis. 2012; 1:133–138. [PubMed: 24729954]
8. Dudley AC, et al. Calcification of multipotent prostate tumor endothelium. Cancer Cell. 2008; 14:201–211. [PubMed: 18772110]
9. Ghosh K, et al. Tumor-derived endothelial cells exhibit aberrant Rho-mediated mechanosensing and abnormal angiogenesis in vitro. Proceedings of the National Academy of Sciences. 2008; 105:11305–11310.
10. St Croix B, et al. Genes expressed in human tumor endothelium. Science. 2000; 289:1197–1202. [PubMed: 10947988]
11. Hida K, et al. Tumor-associated endothelial cells with cytogenetic abnormalities. Cancer Res. 2004; 64:8249–8255. [PubMed: 15548691]
12. Hellebrekers DMEI, et al. Identification of epigenetically silenced genes in tumor endothelial cells. Cancer Res. 2007; 67:4138–4148. [PubMed: 17483324]
13. Soda Y, et al. From the Cover: Feature Article: Transdifferentiation of glioblastoma cells into vascular endothelial cells. Proceedings of the National Academy of Sciences. 2011; 108:4274–4280.
14. Ricci-Vitiani L, Pallini R, Biffoni M, Todaro M. Tumour vascularization via endothelial differentiation of glioblastoma stem-like cells. Nature. 201010.1038/nature09557
15. Wang R, et al. Glioblastoma stem-like cells give rise to tumour endothelium. Nature. 2010; 468:829–833. [PubMed: 21102433]
16. Maniotis AJ, et al. Vascular channel formation by human melanoma cells in vivo and in vitro: vasculogenic mimicry. Am J Pathol. 1999; 155:739–752. [PubMed: 10487832]
17. van der Schaft DWJ. Tumor Cell Plasticity in Ewing Sarcoma, an Alternative Circulatory System Stimulated by Hypoxia. Cancer Res. 2005; 65:11520–11528. [PubMed: 16357161]
18. Pardali E, et al. Critical role of endoglin in tumor cell plasticity of Ewing sarcoma and melanoma. Oncogene. 2011; 30:334–345. [PubMed: 20856203]
19. Cheng L, et al. Glioblastoma Stem Cells Generate Vascular Pericytes to Support Vessel Function and Tumor Growth. Cell. 2013; 153:139–152. [PubMed: 23540695]
20. Sood AK, et al. Molecular Determinants of Ovarian Cancer Plasticity. Am J Pathol. 2001; 158:1279–1288. [PubMed: 11290546]
21. Harrell JC, et al. Endothelial-like properties of claudin-low breast cancer cells promote tumor vascular permeability and metastasis. Clin Exp Metastasis. 201310.1007/s10585-013-9607-4
22. Lai CY, Schwartz BE, Hsu MY. CD133+ Melanoma Subpopulations Contribute to Perivascular Niche Morphogenesis and Tumorigenicity through Vasculogenic Mimicry. Cancer Res. 2012; 72:5111–5118. [PubMed: 22865455]
23. Seftor REB, et al. Tumor cell vasculogenic mimicry: from controversy to therapeutic promise. American Journal Of Pathology. 2012; 181:1115–1125. [PubMed: 22944600]
24. McDonald DM, Munn L, Jain RK. Vasculogenic mimicry: how convincing, how novel, and how significant? Am J Pathol. 2000; 156:383–388. [PubMed: 10666365]
25. van Beijnum JR, Rousch M, Castermans K, van der Linden E, Griffioen AW. Isolation of endothelial cells from fresh tissues. Nat Protoc. 2008; 3:1085–1091. [PubMed: 18546599]
26. Hendrix MJC, Seftor EA, Hess AR, Seftor REB. Vasculogenic mimicry and tumour-cell plasticity: lessons from melanoma. Nat Rev Cancer. 2003; 3:411–421. [PubMed: 12778131]
27. Francescone R, et al. Glioblastoma-derived tumor cells induce vasculogenic mimicry through Flk-1 protein activation. Journal of Biological Chemistry. 2012; 287:24821–24831. [PubMed: 22654102]

28. Xiao L, Harrell JC, Perou CM, Dudley AC. Identification of a stable molecular signature in mammary tumor endothelial cells that persists in vitro. Angiogenesis. 201310.1007/s10456-013-9409-y
29. Kendal WS, Wang RY, Hsu TC, Frost P. Rate of generation of major karyotypic abnormalities in relationship to the metastatic potential of B16 murine melanoma. Cancer Res. 1987; 47:3835–3841. [PubMed: 3594440]
30. Hu FN, Wang RY, Hsu TC. Clonal origin of metastasis in B16 murine melanoma: a cytogenetic study. J Natl Cancer Inst. 1987; 78:155–163. [PubMed: 3467124]
31. DeLisser HM, et al. Involvement of endothelial PECAM-1/CD31 in angiogenesis. Am J Pathol. 1997; 151:671–677. [PubMed: 9284815]
32. Cao G, et al. Involvement of human PECAM-1 in angiogenesis and in vitro endothelial cell migration. Am J Physiol, Cell Physiol. 2002; 282:C1181–90. [PubMed: 11940533]
33. DeLisser H, et al. Vascular endothelial platelet endothelial cell adhesion molecule 1 (PECAM-1) regulates advanced metastatic progression. Proceedings of the National Academy of Sciences. 2010; 107:18616–18621.
34. Dankort D, et al. Braf(V600E) cooperates with Pten loss to induce metastatic melanoma. Nat Genet. 2009; 41:544–552. [PubMed: 19282848]
35. Hanna SC, et al. HIF1α and HIF2α independently activate SRC to promote melanoma metastases. J Clin Invest. 2013; 123:2078–2093. [PubMed: 23563312]
36. Eyles J, et al. Tumor cells disseminate early, but immunosurveillance limits metastatic outgrowth, in a mouse model of melanoma. J Clin Invest. 2010; 120:2030–2039. [PubMed: 20501944]
37. Gessner RC, Aylward SR, Dayton PA. Mapping microvasculature with acoustic angiography yields quantifiable differences between healthy and tumor-bearing tissue volumes in a rodent model. Radiology. 2012; 264:733–740. [PubMed: 22771882]
38. Lin EY, et al. Macrophages regulate the angiogenic switch in a mouse model of breast cancer. Cancer Res. 2006; 66:11238–11246. [PubMed: 17114237]
39. Gumina RJ, Kirschbaum NE, Piotrowski K, Newman PJ. Characterization of the human platelet/endothelial cell adhesion molecule-1 promoter: identification of a GATA-2 binding element required for optimal transcriptional activity. Blood. 1997; 89:1260–1269. [PubMed: 9028949]
40. Roland CL, et al. Inhibition of vascular endothelial growth factor reduces angiogenesis and modulates immune cell infiltration of orthotopic breast cancer xenografts. Mol Cancer Ther. 2009; 8:1761–1771. [PubMed: 19567820]
41. Sullivan LA, et al. r84, a novel therapeutic antibody against mouse and human VEGF with potent anti-tumor activity and limited toxicity induction. PLoS ONE. 2010; 5:e12031. [PubMed: 20700512]
42. Carson C, et al. A prognostic signature of defective p53-dependent G1 checkpoint function in melanoma cell lines. Pigment Cell Melanoma Res. 2012; 25:514–526. [PubMed: 22540896]
43. Hendrix MJ, et al. Expression and functional significance of VE-cadherin in aggressive human melanoma cells: role in vasculogenic mimicry. Proc Natl Acad Sci USA. 2001; 98:8018–8023. [PubMed: 11416160]
44. Huang S, Jean D, Luca M, Tainsky MA, Bar-Eli M. Loss of AP-2 results in downregulation of c-KIT and enhancement of melanoma tumorigenicity and metastasis. EMBO J. 1998; 17:4358–4369. [PubMed: 9687504]
45. Jean D, et al. Loss of AP-2 results in up-regulation of MCAM/MUC18 and an increase in tumor growth and metastasis of human melanoma cells. J Biol Chem. 1998; 273:16501–16508. [PubMed: 9632718]
46. Karjalainen JM, Kellokoski JK, Eskelinen MJ, Alhava EM, Kosma VM. Downregulation of transcription factor AP-2 predicts poor survival in stage I cutaneous malignant melanoma. 1998; 16:3584–3591.
47. Pellikainen J, et al. Reduced nuclear expression of transcription factor AP-2 associates with aggressive breast cancer. 2002; 8:3487–3495.
48. Warren BA, Shubik P. The growth of the blood supply to melanoma transplants in the hamster cheek pouch. Lab Invest. 1966; 15:464–478. [PubMed: 5932611]

49. McDonald DM, Choyke PL. Imaging of angiogenesis: from microscope to clinic. Nat Med. 2003; 9:713–725. [PubMed: 12778170]
50. Yang S, Graham J, Kahn JW, Schwartz EA, Gerritsen ME. Functional roles for PECAM-1 (CD31) and VE-cadherin (CD144) in tube assembly and lumen formation in three-dimensional collagen gels. Am J Pathol. 1999; 155:887–895. [PubMed: 10487846]
51. Dejana E, Orsenigo F, Molendini C, Baluk P, McDonald DM. Organization and signaling of endothelial cell-to-cell junctions in various regions of the blood and lymphatic vascular trees. Cell Tissue Res. 2009; 335:17–25. [PubMed: 18855014]
52. Chang YS, et al. Mosaic blood vessels in tumors: frequency of cancer cells in contact with flowing blood. Proc Natl Acad Sci USA. 2000; 97:14608–14613. [PubMed: 11121063]
53. Di Tomaso E, et al. Mosaic tumor vessels: cellular basis and ultrastructure of focal regions lacking endothelial cell markers. Cancer Res. 2005; 65:5740–5749. [PubMed: 15994949]
54. Sun J, et al. Contributions of the extracellular and cytoplasmic domains of platelet-endothelial cell adhesion molecule-1 (PECAM-1/CD31) in regulating cell-cell localization. J Cell Sci. 2000; 113 (Pt 8):1459–1469. [PubMed: 10725228]
55. Tang DG, Chen YQ, Newman PJ, Shi L, Gao X. Identification of PECAM-1 in solid tumor cells and its potential involvement in tumor cell adhesion to endothelium. Journal of Biological. 1993
56. Peinado H, et al. Melanoma exosomes educate bone marrow progenitor cells toward a pro-metastatic phenotype through MET. Nat Med. 2012; 18:883–891. [PubMed: 22635005]
57. Dudley AC, et al. Bone marrow is a reservoir for proangiogenic myelomonocytic cells but not endothelial cells in spontaneous tumors. Blood. 2010; 116:3367–3371. [PubMed: 20453162]
58. Streeter JE, Gessner R, Miles I, Dayton PA. Improving sensitivity in ultrasound molecular imaging by tailoring contrast agent size distribution: in vivo studies. Mol Imaging. 2010; 9:87–95. [PubMed: 20236606]
59. Kogan P, et al. Validation of dynamic contrast-enhanced ultrasound in rodent kidneys as an absolute quantitative method for measuring blood perfusion. Ultrasound Med Biol. 2011; 37:900–908. [PubMed: 21601135]
60. Roland CL, et al. Cytokine levels correlate with immune cell infiltration after anti-VEGF therapy in preclinical mouse models of breast cancer. PLoS ONE. 2009; 4:e7669. [PubMed: 19888452]

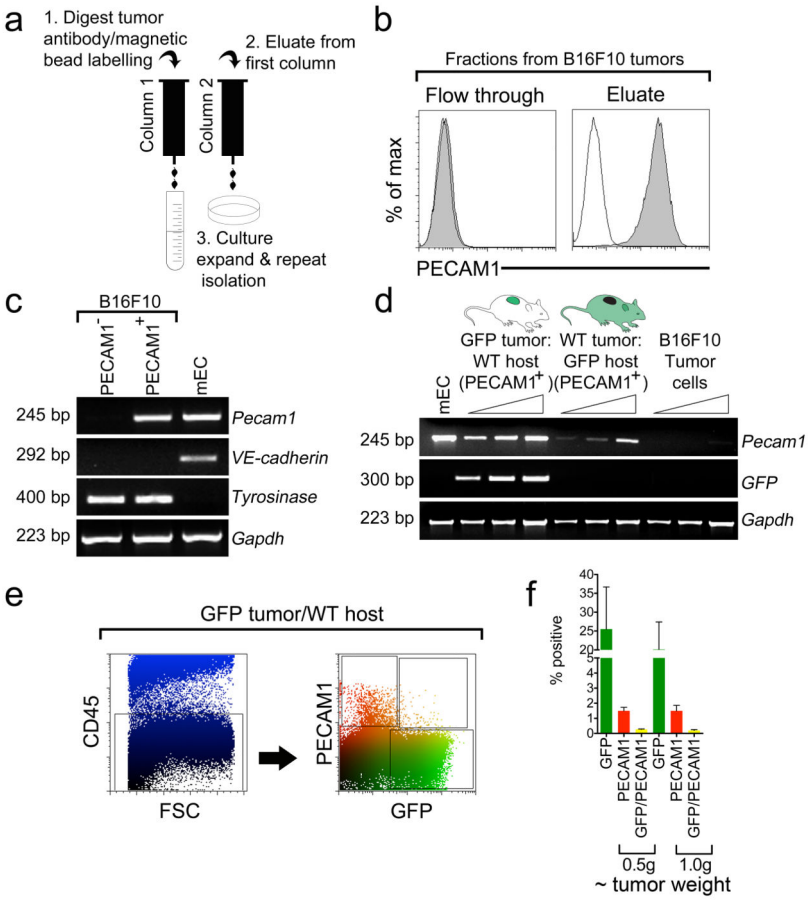

Figure 1. Identification, isolation, and characterization of PECAM1$^+$ tumor cells from B16F10 melanoma

(a) PECAM1 antibodies coupled to immunomagnetic beads were used to enrich PECAM1$^+$ tumor cells from collagenase-digested B16F10 tumors. (b) The enriched cells (eluate) are ~ 99% PECAM1$^+$ by flow cytometry. (c) Purity of the cells was further confirmed by semi-quantitative RT-PCR. The PECAM1$^+$ fraction from B16F10 expresses *Pecam1* and *Tyr*, but not *VE-cadherin*. (d) Retrieval of PECAM1$^+$/GFP$^+$ cells from GFP tumors engrafted in WT hosts and PECAM1$^+$/GFP$^-$ cells engrafted in GFP hosts. Following immunomagnetic separation with PECAM1 antibodies, increasing amounts of cDNA template were analyzed by semi-quantitative RT-PCR, indicated by the wedge. (e) Detection of PECAM1$^+$/GFP$^+$ tumor cells in vivo after injecting B16F10-GFP tumor cells into WT hosts. CD45$^+$ hematopoietic cells were excluded by out-gating. The upper right quadrant are PECAM1$^+$ tumor cells which comprise ~ 0.1% of each tumor. (f) The percentage of PECAM1$^+$/GFP$^+$ tumor cells are shown for two time points when tumors were different sizes (n = 3 mice per group). (error bars = s.e.m.)

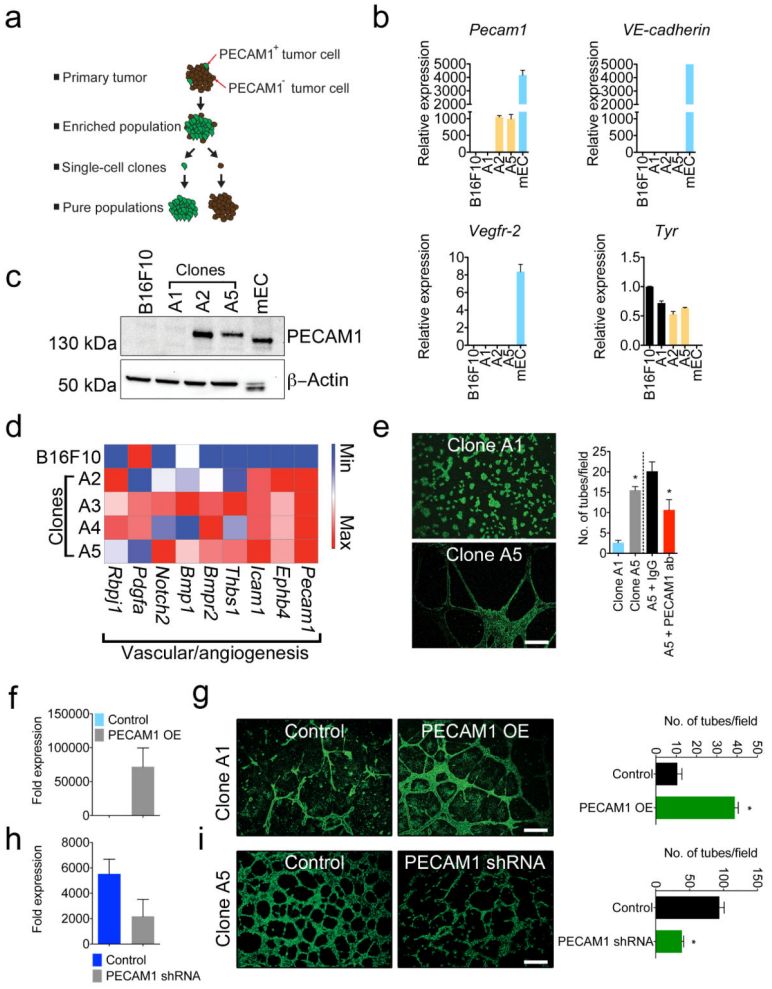

Figure 2. PECAM1$^+$ clonally-derived populations from B16F10 melanoma display vascular characteristics and form PECAM1-dependent tube-like structures

(a) Strategy for preparation of PECAM1$^+$ clonal populations from B16F10 melanoma using limiting dilutions of partially-enriched cellular fractions. (b) Characterization of PECAM1$^-$ and PECAM1$^+$ clonal populations using qPCR. (c) Western blotting for PECAM1 using whole cell extracts from the indicated cell type. PECAM1 migrates at the expected size of ~ 130 kDa. Blots were stripped and re-probed with β-actin antibodies to show equal loading. (d) Microarray analysis of parental B16F10 and PECAM1$^+$ clonal populations derived from B16F10. Only known vascular or angiogenesis-related genes shown to be up-regulated in PECAM1$^+$ clones are shown. (e) Images from tube-forming assay in Matrigel comparing a PECAM1$^-$ (A1) and PECAM1$^+$ (A5) clone. Tube-like structures in high power fields were quantified and plotted. Sample means were statistically significant as determined by a Student's t-test ($p<0.02$, n = 6 wells per condition). (f) qPCR analysis of *Pecam1* expression in PECAM1$^-$ melanoma cells (clone A1) following ectopic PECAM1 expression. (g) Images of control-transfected cells and PECAM1 over-expressing cells (OE) are shown after a 16-hour tube formation assay and quantified at right. Means are statistically significant as determined by a Student's t-test ($p<0.001$, n = 6–7 wells per condition). (h) qPCR analysis of *Pecam1* expression in PECAM1$^+$ melanoma cells (clone A5) following shRNA

knockdown. (i) Images of empty-vector transfected and *Pecam1* shRNA-transfected cells are shown after a 16-hour tube formation assay and quantified at right. Means are statistically significant as determined by a Student's t-test ($p<0.001$, $n = 7–8$ wells per condition). (scale bars = 100 μm, error bars = s.e.m.)

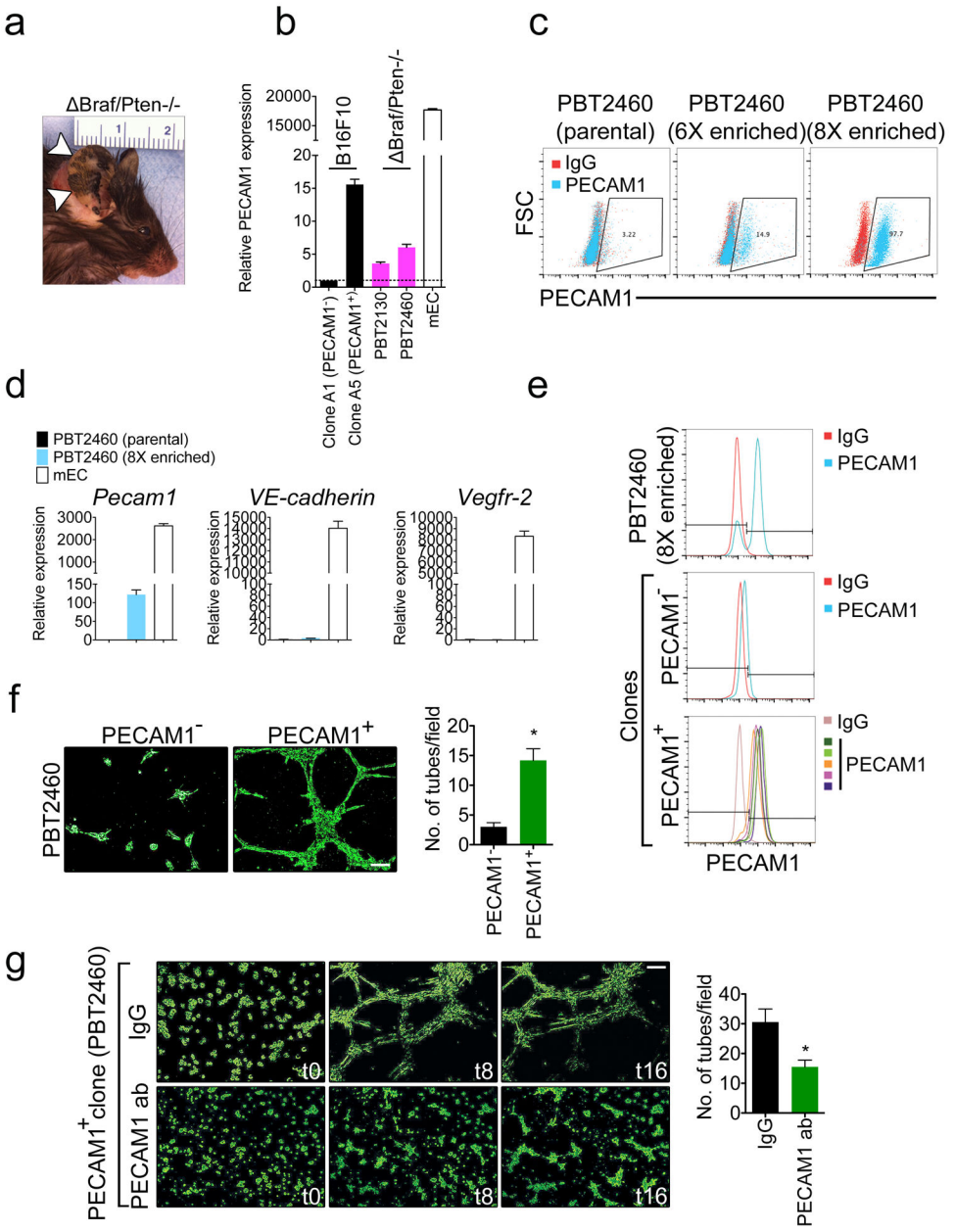

Figure 3. PECAM1^{+}/VEGFR-2^{-} tumor cells exist in a genetically engineered mouse model of melanoma and they form vascular-like networks in Matrigel

(a) Examples of tumors from ΔBraf/Pten−/− mice. (b) qPCR analysis of *Pecam1* expression in PECAM1^{-} and PECAM1^{+} B16F10 clonal populations and two additional unsorted cell lines derived from dispersed tumors from ΔBraf/Pten−/−mice. mEC are a positive control for *Pecam1* expression. (c) Flow cytometry analysis of unsorted (parental) PBT2460 cells shows ~ 3% positivity for PECAM1. After six rounds of PECAM1 selection, this fraction increases to ~ 15% and after eight rounds to ~ 98%. (d) qPCR analysis of the parental PBT2460 population versus the 8X-enriched fraction. Basal *Pecam1* expression is ~ 100-fold higher in the 8X-enriched fraction compared to unsorted PBT2460 cells, while neither population expresses *VE-cadherin* or *Vegfr-2*. (e) Using the 8X-enriched fraction, single cell

clones were prepared by limiting dilution assays and then analyzed by flow cytometry for PECAM1 expression. (f) Clonally-derived PECAM1^{+} PBT2460 cells show an ~ 5-fold increase in tube formation as compared to PECAM1^{-} cells. Sample means were statistically significant as determined by a Student's t-test ($p<0.0001$). (g) Time-lapse images of tube formation assay using clonally-derived PECAM1^{+} PBT2460 cells incubated with either a non-specific IgG (top row) or PECAM1-blocking antibody (bottom row). Elapsed time is shown in hours. At right: PECAM1 blocking antibodies reduce tube formation by ~ 50% in PECAM1^{+} PBT2460 cells. Sample means were statistically significant as determined by a Student's t-test ($p<0.01$). (scale bars = 100 μm, error bars = s.e.m.)

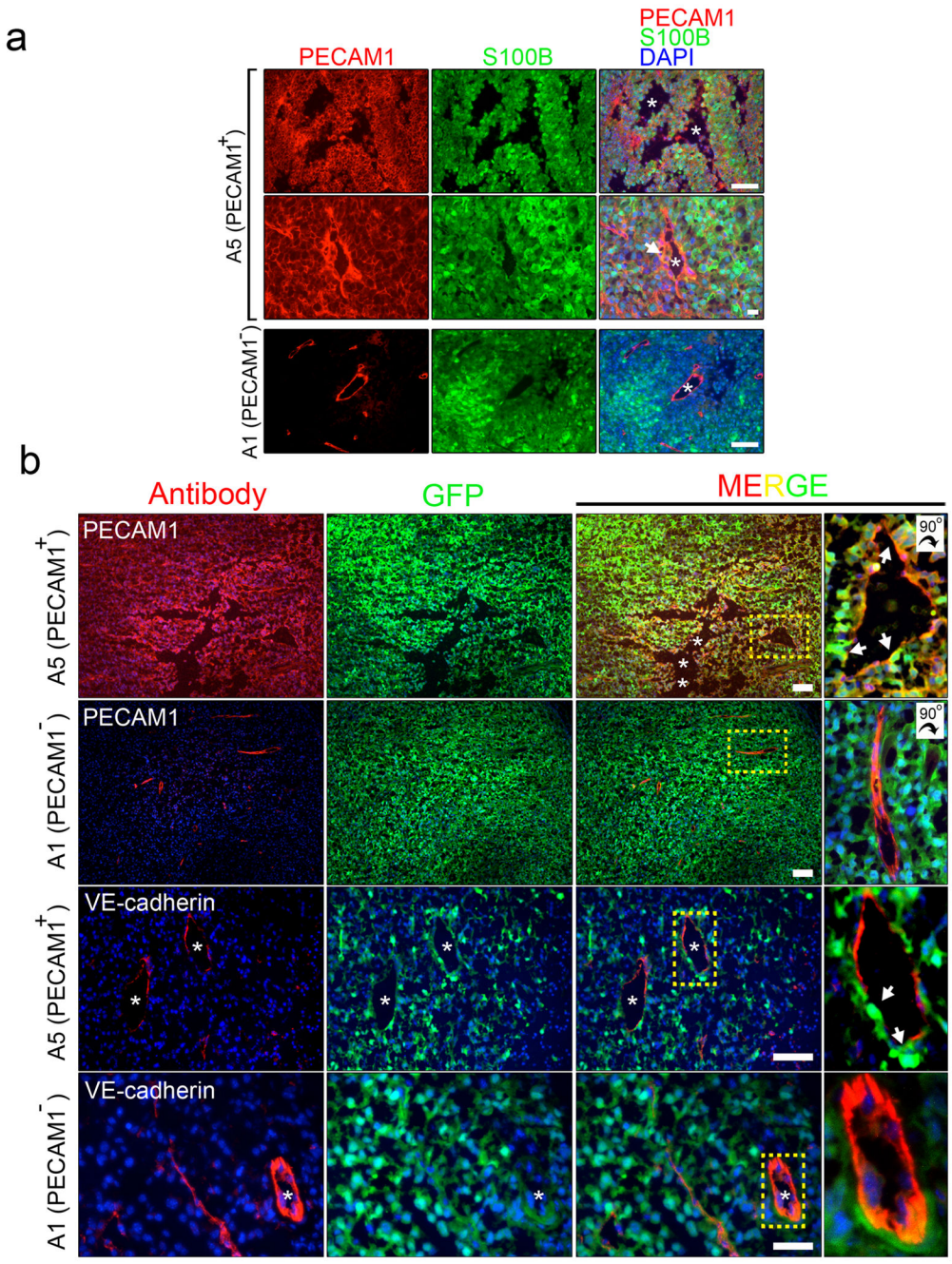

Figure 4. PECAM1$^+$ melanoma cells integrate within vessel lumens in vivo

(a) Engraftment of unlabeled PECAM1$^-$ (clone A1) and PECAM1$^+$ (clone A5) tumor cells in C57BL6/J mice. Tumors were implanted subcutaneously and then harvested ~ 3 weeks later. Frozen sections were stained with PECAM1 and S100b antibodies. Asterisks indicate blood vessels. Arrows show luminally-positioned tumor cells. (b) Representative GFP-labeled PECAM1$^+$ and PECAM1$^-$ tumors are shown. Sections were stained with PECAM1 or VE-Cadherin antibodies where indicated. The boxed regions shown at far right are zoomed regions taken from these images. In the top panels, asterisks indicate tumor cell-lined “channels”. The arrows show luminally-positioned tumor cells. In the bottom panels,

the asterisks and arrows indicate where host-derived VE-cadherin^{+} EC are absent but void space is filled by GFP^{+}/PECAM1^{+} tumor cells. In PECAM1^{-}/GFP^{+} tumors shown for comparison, PECAM1^{-}/GFP^{+} tumor cells surround a host-derived, VE-cadherin^{+} vessel but do not incorporate into the lumen. (long scale bars = 100 μm, short = 20 μm)

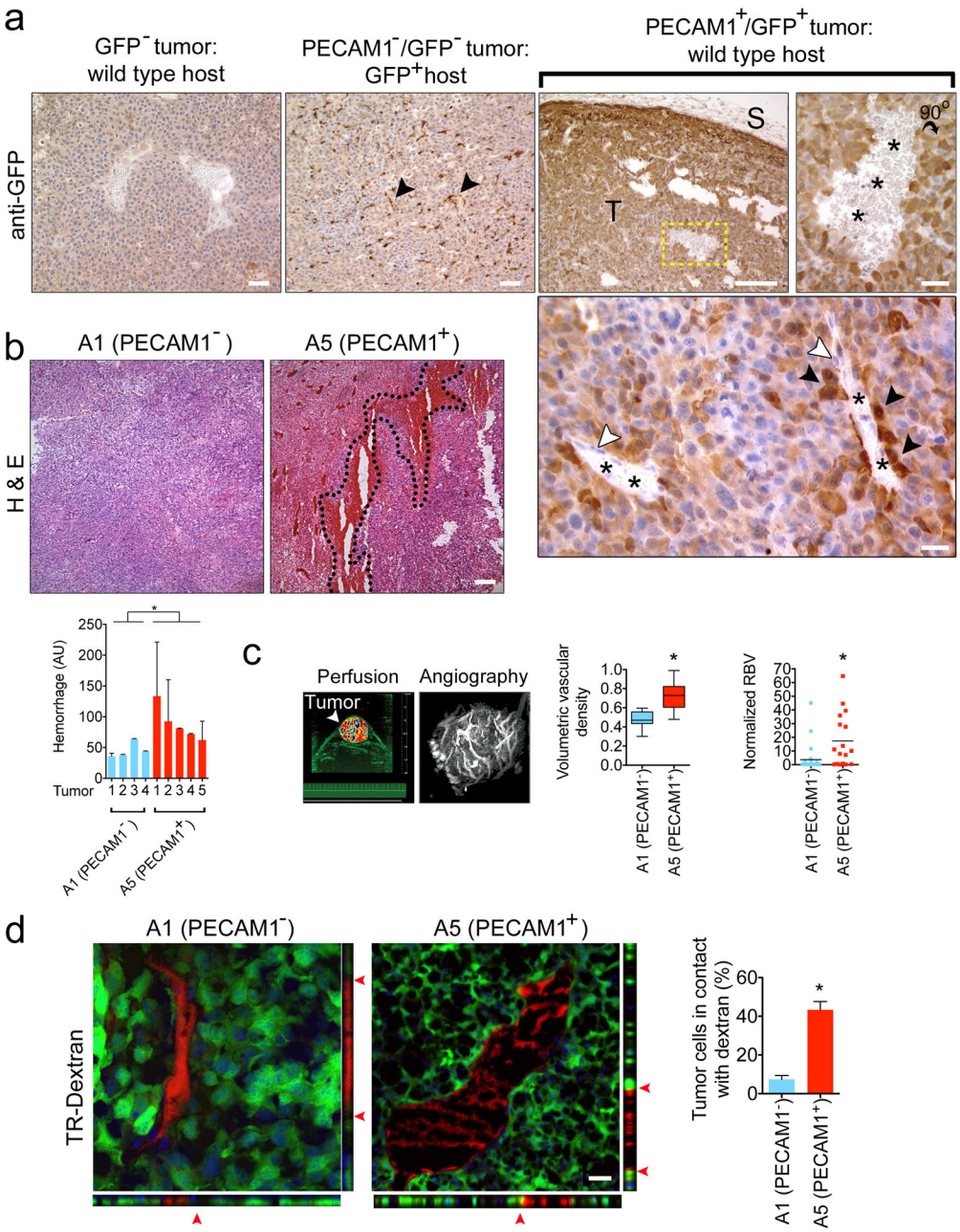

Figure 5. PECAM1$^+$ melanoma cells form primitive but perfused vascular structures

(a) 3,3′ diaminobenzidine (DAB) detection of GFP antibodies used to stain tumors. Unlabeled B16F10 tumors implanted in wild type hosts were used as negative controls. Blood vessels are visible in the center of field. Unlabeled PECAM1$^-$ tumors implanted in a GFP host showed an expected staining pattern of host-derived blood vessels (black arrow heads) and stromal cells. PECAM1$^+$/GFP$^+$ tumor cells contained large “holes” and channels, some of which were blood-filled. GFP$^+$ tumor cells in right two panels appear to be in direct contact with red blood cells (asterisks). The boxed area in the third panel is magnified on far right. Tumor area is marked with a “T” and the overlying mouse skin (GFP$^-$) is marked with an “S.” Lower panel shows a second PECAM1$^+$ clone (clone A2) with PECAM1$^+$/GFP$^+$

tumor cells closely aligned with host blood vessels. Some unstained endothelial cell nuclei are also visible and are marked with white arrowheads. (b) H & E stained sections of PECAM1^{-} and PECAM1^{+} tumors reveals large areas of hemorrhage and vessel dilation. Tumor sections were analyzed using ImageJ and are plotted. Sample means were statistically significant as determined by a Student's t-test ($p=0.0384$, $n = 5$ tumors). (c) Tumor vascularity was measured using 3D acoustic angiography imaging. Means were statistically significant using a Welch two sample t-test ($p=0.003$, $n = 9$ for PECAM1^{-} tumors and $n = 8$ for PECAM1^{+} tumors). Area-normalized relative blood volume was calculated from 2D destruction-reperfusion imaging. A linear mixed-effects model was used to calculate statistical significance ($p=0.0182$). (d) TR-Dextran was injected intravenously in mice bearing GFP-labeled PECAM1^{-} or PECAM1^{+} tumors. Harvested tumors were sectioned and imaged on a confocal microscope. Red arrowheads point to GFP^{+}/TR-Dextran^{+} areas. Ten separate fields from tissue sections from each mouse were used to quantify number of tumor cells in contact with the circulation as shown. Means were statistically significant using an unpaired two tailed t-test, ($p < 0.0001$, $n = 4$). (scale bars = 100 μm, short bars in high-magnification panels = 20 μm, error bars = s.e.m.)

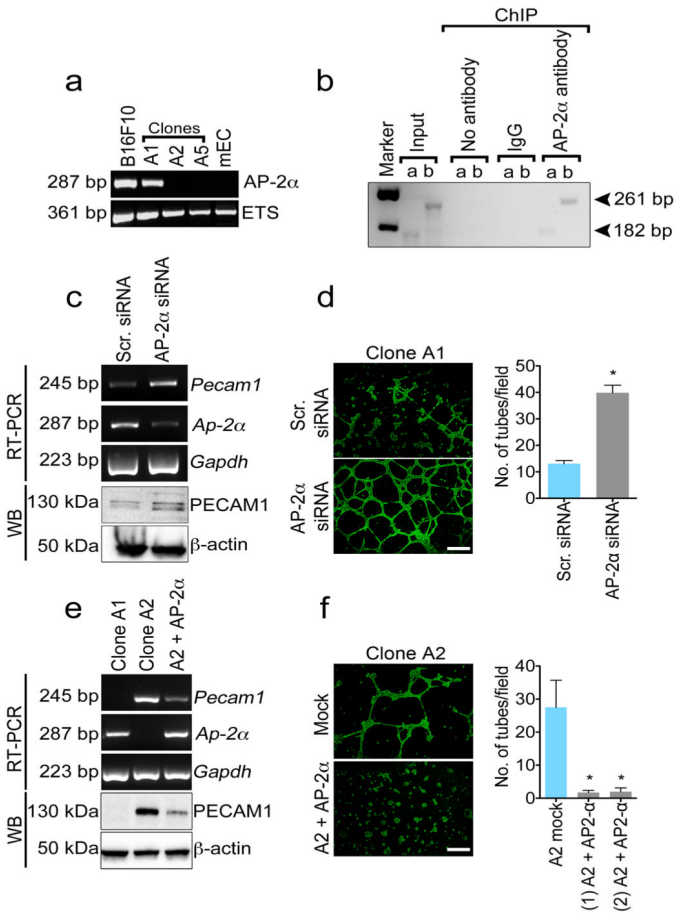

Figure 6. AP-2α is diminished in PECAM1$^+$ tumor cells and is a transcriptional repressor of PECAM1

(a) Semi-quantitative RT-PCR analysis of *Ap-2α* and *Ets* transcription factors in PECAM1$^-$ and PECAM1$^+$ clones. (b) Chromatin immunoprecipitation using B16F10 tumor cells. Purified genomic DNA was incubated with AP-2α antibodies followed by capture on protein-G agarose. Samples were analyzed by semiquantitative RT-PCR using two primer sets predicted to amplify different regions of the mouse *Pecam1* promoter (indicated by arrow heads). (c) siRNA knockdown of *Ap-2α*. Cells were incubated for 48 hours with 100 nM of either scrambled control (Scr. siRNA) or *Ap-2α* siRNA. Cell extracts were then evaluated by RT-PCR and western blotting. (d) Images of tube forming assay in a PECAM1$^-$ clone following *Ap-2α* siRNA knockdown. Images were taken approximately 16 hours after seeding on Matrigel. Quantification of tube-forming ability following *Ap-2α* siRNA knockdown on right. Results are statistically significant where indicated by an asterisk ($p<0.0001$ by unpaired t-test, n = 12 observations from individual wells). (e) Lentiviral over-expression of *Ap-2α* in PECAM1$^+$ clones. Stable cell lines were established from clonal populations following *Ap-2α* introduction and selection in Zeocin. Cell extracts were evaluated by RT-PCR and western blotting. (f) Images of tube forming assay in a PECAM1$^+$ clone following *Ap-2α* lentiviral introduction. Images were taken approximately 16 hours after seeding on Matrigel. Quantification of tube-forming ability following *Ap-2α* lentiviral introduction on right. Results are statistically significant where indicated by an

asterisk and were confirmed using two different derived clones (p=0.0202, n = 3–4 observations from individual wells). (scale bars = 100 μm, error bars = s.e.m.)

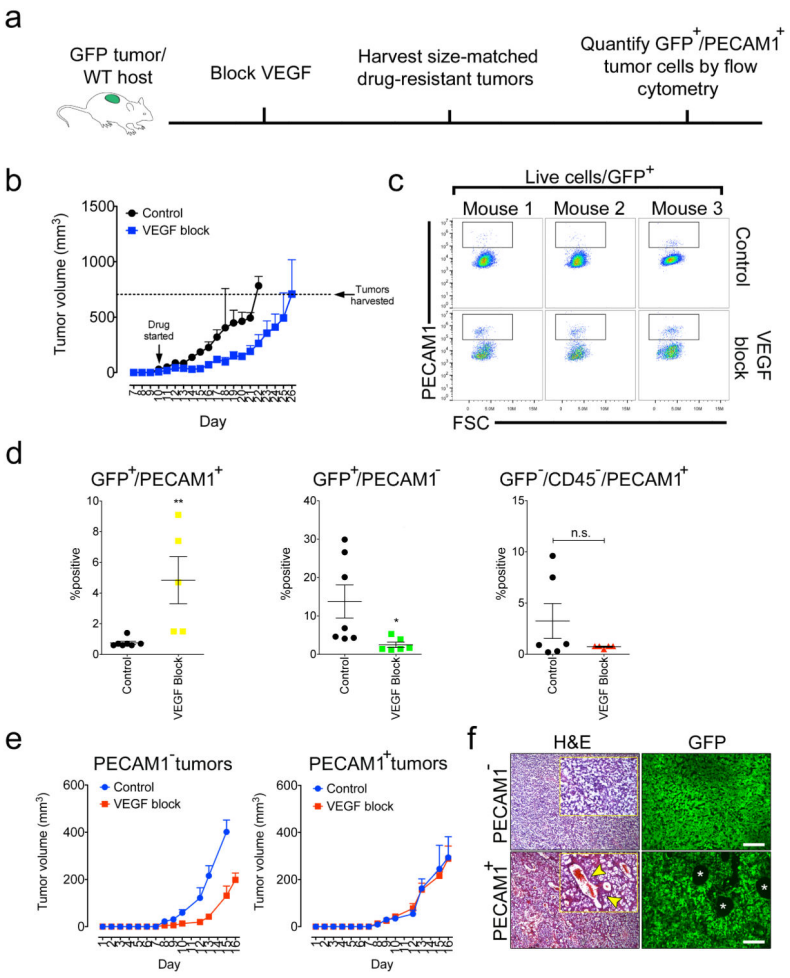

Figure 7. PECAM1$^+$ tumor cells are enriched in tumors challenged with anti-VEGF therapy

(a) Experimental design. (b) Tumor volumes in control (n = 8) and MCR84-treated (n = 8) mice measured with calipers each day. MCR84 treatment was initiated where indicated. (c) Flow cytometry analysis of collagenase-dispersed tumors from control and MCR84-treated mice. Three representative dot plots from individual mice are shown. Live cells/GFP$^+$ cells were selected and then gated for PECAM1. The top three panels are controls and the bottom three panels are MCR84-treated mice. (d) Quantification of tumor subpopulations from collagenase-dispersed tumors using flow cytometry (n = 5–7 mice/group). Results are statistically significant where indicated with an asterisk (left, p=0.0095; center, p=0.0361; right, n.s. = not significant) as evaluated by Student's t-test. (e) Tumor growth in mice bearing PECAM1$^-$ tumors (clone A1) or PECAM1$^+$ tumors (clone A5) challenged with MCR84. Drug treatment was initiated on day five and tumor sizes were measured each day with calipers (n = 4–5 mice per group). (f) H & E and GFP-stained tissue sections from MCR84-treated PECAM1$^-$ and PECAM1$^+$ tumors. Zoomed regions (yellow insets) demonstrate dense pockets of PECAM1$^+$ tumor cells surrounding a vessel lumen (also identified by asterisks in the accompanying GFP-stained section). (scale bars = 100 μm, error bars = s.e.m.)

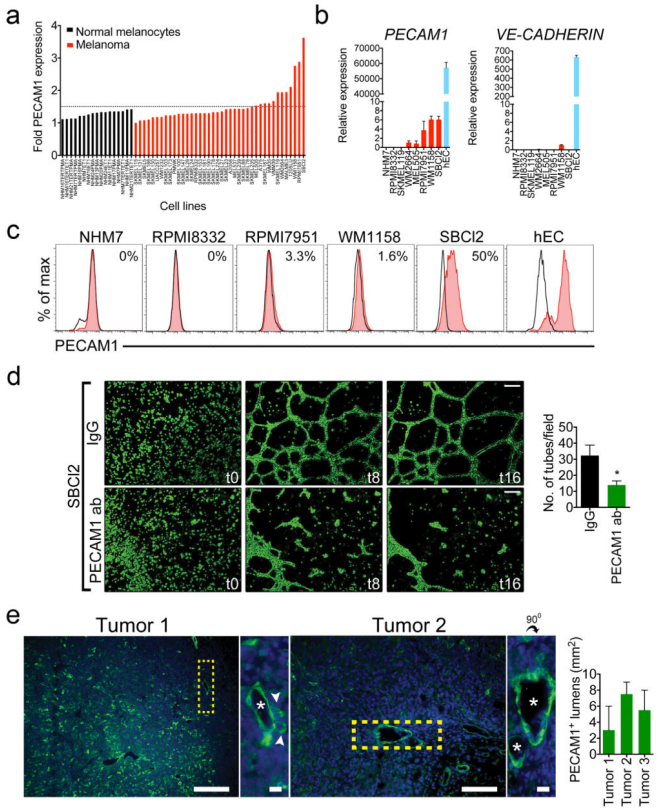

Figure 8. Human melanoma contains a PECAM1$^+$ subpopulation that displays vascular-like characteristics

(a) Microarray analysis of normal human melanocytes (black bars) and human melanoma (red bars). Each cell line and the raw fluorescence intensity value from the microarray are listed in Supplementary Table 2. The dotted horizontal line on the graph is the threshold below which no *PECAM1* transcripts are detected. (b) Quantitative real-time PCR analysis of *PECAM1* and *VE-CADHERIN* expression in normal melanocytes and seven of the highest *PECAM1*-expressing cell lines predicted from the microarray. Except for WM1158, no *VE-CADHERIN* transcripts were detected. Human endothelial cells (hEC) were used as a positive control. (c) Flow cytometry of selected cell lines stained with human-specific PECAM1 antibodies. (d) Time-lapse images of tube formation assay using the PECAM1$^+$ human melanoma cell line SBCl2 incubated with either a non-specific IgG (top row) or PECAM1-blocking antibody (bottom row). Far right: PECAM1 blocking antibodies reduce tube formation by ~ 60% in PECAM1$^+$ SBCl2 cells. Sample means were statistically significant as determined by a Student's t-test ($p=0.02$, $n = 8$ wells per condition). (e) PECAM1$^+$ lumens formed by SBCl2 tumors. The asterisks mark lumens and white arrow head shows PECAM1$^+$ tumor cells positioned at the abluminal surface. Two sections from each tumor were scanned for PECAM1$^+$ lumens and the mean values were plotted on right. (scale bars = 100μm, short bars in high-magnification panels = 20 μm, error bars = s.e.m.)

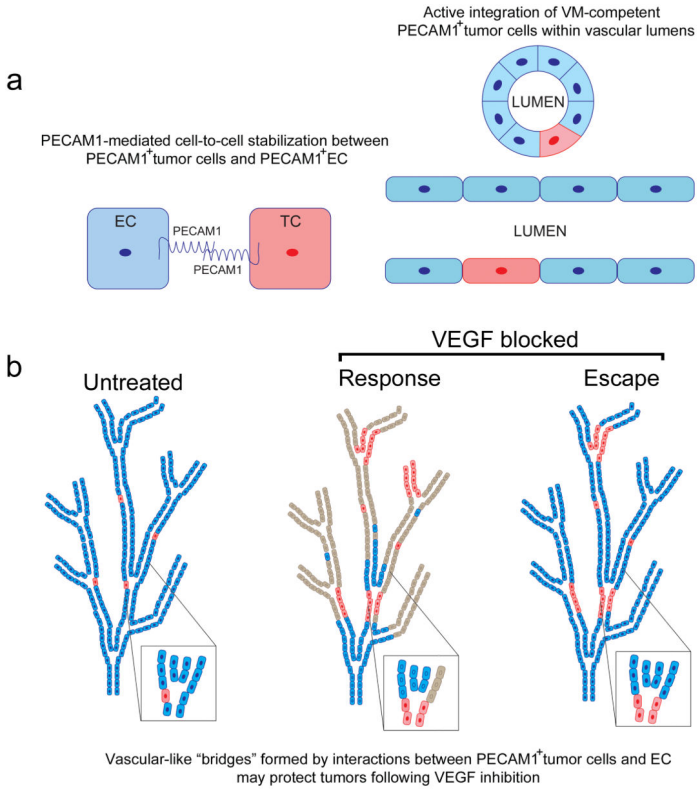

Figure 9. A model for a PECAM1-dependent form of vasculogenic mimicry

(a) PECAM1 plays a well-characterized role in stabilizing junctions between EC and leukocytes and between two EC. Tumor cell expression of PECAM1 may also stabilize interactions between tumor cells (TC) and EC or between two PECAM1$^+$ TC to form stable junctions. (b) In tumors where PECAM1$^+$ tumor cells are present, VEGF-independent "bridges" would not be affected by anti-VEGF therapies and could supplant host endothelium following VEGF inhibition. "Channels" formed exclusively by PECAM1$^+$ TC could also be insensitive to VEGF blockade.